Mechanisms of Glycerol Dehydration

Mark R. Nimlos,*,† Stephen J. Blanksby,‡ Xianghong Qian,§ Michael E. Himmel,† and David K. Johnson†

National Bioenergy Center, National Renewable Energy Laboratory, Golden, Colorado 80401, U.S.A., Department of Chemistry, University of Wollongong, Wollongong, NSW 2522, Australia, and Rx-Innovation, Inc., Fort Collins, Colorado 80525, U.S.A.

Received: January 27, 2006; In Final Form: March 6, 2006

Dehydration of neutral and protonated glycerol was investigated using quantum mechanical calculations (CBS-QB3). Calculations on neutral glycerol show that there is a high barrier for simple 1,2-dehydration, E_a = 70.9 kcal mol^{-1}, which is lowered to 65.2 kcal mol^{-1} for pericyclic 1,3-dehydration. In contrast, the barriers for dehydration of protonated glycerol are much lower. Dehydration mechanisms involving hydride transfer, pinacol rearrangement, or substitution reactions have barriers between 20 and 25 kcal mol^{-1}. Loss of water from glycerol via substitution results in either oxirane or oxetane intermediates, which can interconvert over a low barrier. Subsequent decomposition of these intermediates proceeds via either a second dehydration step or loss of formaldehyde. The computed mechanisms for decomposition of protonated glycerol are supported by the gas-phase fragmentation of protonated glycerol observed using a triple−quadrupole mass spectrometer.

Introduction

Carbohyhdrates are major constituents of plant cell walls, and an understanding of their chemistry plays an important role in botany and energy sciences. Of increased recent interest is the use of sugars from plant matter as a renewable source of energy, fuels, and chemicals.[1−5] In many scenarios, extracting the sugars from plant cell walls without further degradation is crucial to the viability of the technology. Additionally, the use of sugars as a feedstock for the formation of chemicals and fuels is being explored. In both cases, understanding the mechanisms and kinetics of sugar chemistry is essential.

Mechanistic studies of sugars are difficult, however, because of the complexity arising from numerous adjacent (vicinal) hydroxyl groups. As is often the case in other systems, some of the important chemistry of sugars can be explored by studying smaller, structurally similar molecules. Glycerol (1,2,3-propanetriol) provides such a model because of its three adjacent hydroxyl groups and because it is a small enough molecule that it can be modeled with high accuracy using available computational methods.

Pyrolysis of glycerol has been studied in steam[6,7] and supercritical water[8,9] with acrolein (2-propenal), formaldehyde (methanal), and acetaldehyde (ethanal) observed as the major products at lower temperatures. These products appear to result from dehydration and fragmentation of glycerol. At higher temperatures, other products such as carbon dioxide, molecular hydrogen, ethylene, and methane are observed, indicative of more complex chemistry. Mechanisms were proposed for the formation of these products, and complex chemical kinetic models were developed and tested. Unfortunately, the mechanisms, reaction rates, and energetics of many of the reactions of glycerol are unknown. For carbohydrates in aqueous solutions, there is the possibility that protonation could lead to enhanced degradation;[10−14] thus, the unimolecular decompositon of protonated glycerol should also be considered.

Unfortunately, there are few detailed kinetic or mechanistic studies of the decomposition of glycerol or protonated glycerol. However, there have been a number of experimental and theoretical studies of the unimolecular decomposition of protonated diols. These studies show that reactions leading to the loss of one and two water molecules are important. The mechanisms proposed for these reactions include the pinacol rearrangement[15] and substitution processes involving the formation of cyclized products.[16,17] It is not immediately obvious how the additional hydroxyl group in glycerol will influence this chemistry.

In this study, the unimolecular decomposition of neat glycerol and glycerol in the presence of a proton were investigated using molecular modeling. Given the moderate size of the molecular system (6 heavy atoms), the highly accurate quantum mechanical CBS-QB3 computational techniques were utilized. In addition to the calculations, the collisional induced dissociation (CID) mass spectra of protonated glycerol and selected isotopologues were measured using a triple−quadrupole mass spectrometer. These experimental data are discussed in context of the calculations.

Methods

Computational. Calculations were conducted using the Gaussian 98[18] and Gaussian 03[19] suites of programs, running on an IBM RS/6000, an SGI cluster, a SUN Ultra 80, and a MacIntosh G5. Structures of reactants, products, and the transition states (TSs) that connect them were obtained and energies and vibrational frequencies were then determined at these optimized geometries. Activation energies for reactions, E_a, were estimated as the relative energies, including zero-point energies, between the transition state and the reactant, $\Delta_{TS}E_{0K}$. Reactants and products had no imaginary frequencies, whereas transition states had exactly one imaginary frequency. Transition

* To whom correspondence should be addressed. E-mail: mark_nimlos@nrel.gov.
† National Renewable Energy Laboratory.
‡ University of Wollongong.
§ Rx-Innovation, Inc.

10.1021/jp060597q CCC: $33.50
Published on Web 04/18/2006

states were confirmed by visual inspection of the imaginary frequency using Gaussview and by separate IRC calculations. Stable structures and transition states were often initially located using HF/3-21G(d) and then reoptimized using B3LYP/6-311G-(d,p). This level of theory has a quoted accuracy of ±3.0 kcal mol^{-1} for the G2 set of molecules;[20] however, B3LYP is known to often under-predict activation energies[21−24] by up to 5 kcal mol^{-1}. To obtain more accurate energies, we used a complete basis set extrapolation technique (CBS-QB3) developed by Peterson et al.[25] This technique uses geometries optimized at the B3LYP/6-311G(d,p) level and extrapolates to the complete basis set limit at the QCISD level**.** This technique has a quoted accuracy of 1.2 kcal mol^{-1} for the G2 molecule set and has been shown to produce more accurate activation energies than B3LYP.[21,22,26]

Mass Spectrometry. Glycerol, ^{13}C-2-glycerol, $^{13}C_2$-1,3-glycerol, and glycidol were obtained from Sigma-Aldrich (Castle Hill, Australia) and used without purification. Standard solutions of 10 μM were prepared in aqueous acetonitrile (approximately 1:1 by volume) with the pH adjusted to 3 using aqueous formic acid. Mass spectra were obtained using a QuattroMicro triple−quadrupole mass spectrometer (Waters, Manchester, UK) fitted with a Z-spray electrospray ionization source. Protonated analyte ions were obtained by infusion of the standard solution (10 μL/min) into the electrospray source in positive-ion mode. Typical settings were cone voltage = 20 V, capillary voltage = 3 kV, and source temperature = 80 °C. Care was taken with the cone voltage settings to minimize the fragmentation of the protonated alcohols upon extraction into the low-pressure region. ESI-MS spectra were obtained by scanning Q1 while operating Q3 in R_f-only mode. Resolution for ESI-MS and ESI-MS/MS experiments was typically 0.7 Th across the entire mass range. ESI-MS/MS spectra were obtained by mass-selecting the parent ion using Q1 and scanning for product ions using Q3. Argon was used as the collision gas at a pressure of 4×10^{-3} Torr. ESI-MS/MS spectral data presented in this paper result from the average of at least 50 scans. The data were baseline subtracted (40% background subtract with a first-order polynomial) and smoothed (two mean smoothings with a peak width of 0.7 Th) using the MassLynx software (Waters, Manchester UK).

Results and Discussion

Glycerol Structure. In a computational study of dehydration reactions of glycerol, it is important to establish a starting structure for glycerol. There are 126 possible conformers of glycerol, all of which have been characterized in a recent study by Hadad and co-workers using a variety of theories.[27] These authors found that in the lowest energy conformer at the CCSD-(T)/6-31+G(d,p)//HF/6-31G(d) and CBS-QB3 levels, the hydroxyl groups form a cyclic structure with three internal hydrogen bonds. Using the convention of that study, this conformer is termed gG′g,g′Gg ($\gamma\gamma$), and we have used this as the lowest energy conformer and starting point for the present work. All energies for the reactions of neutral glycerol are given relative to this conformer. Figure 1 shows the structure of the gG′g,g′Gg ($\gamma\gamma$) conformer at the B3LYP/6-311G(d,p) level with the internal hydrogen bond lengths indicated. From this starting geometry, two dehydration mechanisms have been considered here: 1,2-dehydration and 1,3-dehydration.

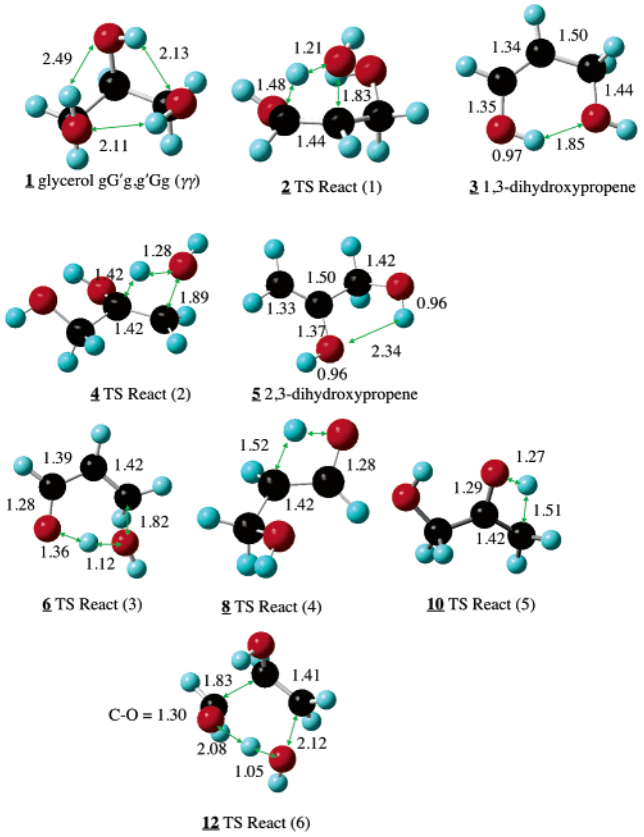

Figure 1. Selected bond lengths in Å for reactants, products, and transition states for dehydration of neutral glycerol as determined with B3LYP/6-311G(d,p).

1,2-Dehydration in Neutral Glycerol. The mechanisms for 1,2-dehydration of glycerol are shown in reactions 1 and 2, where either the central hydroxyl group or a terminal hydroxyl group is lost. As is shown, the transition states for these reactions, **2** and **4**, have four atom centers, and the products are 1,3-dihydroxypropene, **3**, and 2,3-dihydroxypropene, **4**. These reactions are endothermic with energies of $\Delta_{react}E_{0K}$[reaction 1] = 8.5 kcal mol^{-1} and $\Delta_{react}E_{0K}$[reaction 2] = 6.9 kcal mol^{-1}. The lowest-energy conformers of the products have intramolecular hydrogen bonding, and the structures are shown in Figure 1. The transition states for these two reactions are also shown in Figure 1, and the distances between the four atoms involved in dehydration are indicated. Consistent with the convention of dehydration of alcohols, the β H atom is H1 for TS **2** and H2 for TS **4**, whereas the α and β C atoms are C2 and C1 for TS **2** and C1 and C2 for TS **4**. For **2** and **4**, the $C_\beta-H_\beta$ bond lengths are 1.48 and 1.42 Å, the $O-H_\beta$ bond lengths are 1.21 and 1.28 Å, the $C_\beta-C_\alpha$ bond lengths are 1.44 and 1.42 Å, and the $C_\alpha-O$ bond lengths are 1.83 and 1.89 Å. These values are similar to those calculated[22] for the transition states of 1,2-dehydration of simple alcohols; 1.32−1.45 Å for $C_\beta-H_\beta$, 1.26−1.35 Å for $O-H_\beta$, 1.42−1.44 Å for $C_\beta-C_\alpha$, and 1.86−2.08 Å for $C_\alpha-O$. The relative energies of the transition states, $\Delta_{TS}E_{0K}$[reaction 1] = 70.9 kcal mol^{-1} and $\Delta_{TS}E_{0K}$[reaction 2] = 73.2 kcal mol^{-1} are also comparable to the results obtained for simple alcohols. Calculated barriers for the dehydration of a number of alcohols is reported[22] to be 66−70 kcal mol^{-1} and experimental values are 66.2 kcal mol^{-1} for *tert*-butyl alcohol[28] and 64.7 kcal mol^{-1} for 2,3-dimethylbutan-2-ol.[29] Such high energy barriers indicate that these reactions are only likely at high temperatures and under pyrolysis conditions.

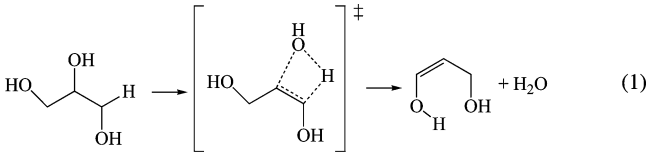

(1)

1 **2** **3**

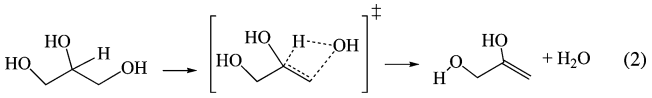

(2)

1 **4** **5**

Further dehydration of 1,3-dihydroxypropene, **3**, can occur by transfer of a proton from the vinyl hydroxyl group to the methyl hydroxy group, as is shown in reaction 3. Because this involves a six-centered transition state, **6**, one would expect a lower-energy transition state, and this is found to be the case with an activation energy of $\Delta_{TS}E_{0K}$[reaction 3] = 29.8 kcal mol^{-1}. This reaction leads to the formation of acrolein, **7**, and is slightly endothermic, $\Delta_{react}E_{0K}$[reaction 3] = 0.8 kcal mol^{-1}. A similar reaction for **5** would require a four-centered transition state and would result in the formation of a diradical, making this process unlikely. The calculated structure of the transition state, **6**, is shown in Figure 1 and is consistent with this pericyclic six-centered mechanism. The O1−H bond has lengthened to r_{O1-H}(**6**) = 1.36 Å, whereas the distance between this hydrogen atom and O3 has shortened to r_{O3-H}(**6**) = 1.12 Å. Furthermore, the C3−O3 bond is nearly broken, r_{O3-O3}(**6**) = 1.82 Å, and the C2−C3 and C1−O1 bonds have developed double-bond character, r_{C2-C3}(**6**) = 1.42 Å and r_{C1-O1}(**6**) = 1.28 Å.

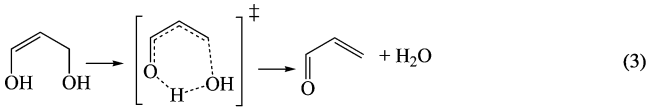

(3)

3 **6** **7**

Keto−enol tautomerism is also possible for the dihydroxypropene products of 1,2-dehydration. Reactions 4 and 5 depict tautomerization of **3** and **5** via the four-centered transition states, **8** and **10**, respectively. The reaction products, 3-hydroxypropenal, **9**, or hydroxyacetone, **11**, are more stable than their enol forms (with reaction exothermicities of $\Delta_{react}E_{0K}$[reaction 4] = −7.8 kcal mol^{-1} and $\Delta_{react}E_{0K}$[reaction 5] = −10.9 kcal mol^{-1}), but the reactions have high barriers, $\Delta_{TS}E_{0K}$[reaction 4] = 60.0 kcal mol^{-1} and $\Delta_{TS}E_{0K}$[reaction 5] = 53.1 kcal mol^{-1}. The barriers for tautomerization are lower than those for dehydration, and reaction 5 should occur. Other tautomeric structures of **5** could exist, i.e., $CH_3C(OH)$=CHOH and $CH_3CH(OH)CHO$, but these would require more extensive rearrangements. However, reaction 4 will not be able to compete with reaction 3, which has a much lower barrier even though the entropy of activation for reaction 4 is $\Delta_{TS}S$ [reaction 4] = 0.7 cal mol^{-1} compared to $\Delta_{TS}S$ [reaction 3] = −4.3 cal mol^{-1}.

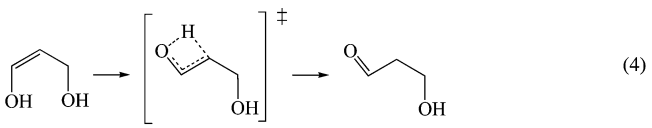

(4)

3 **8** **9**

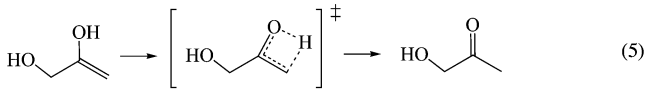

(5)

5 **10** **11**

Potential energy plots for reactions 1−5 are collected in Figure 2. From these results, one can see that the 1,2-dehydration resulting in the loss of the hydroxyl group from the central or terminal carbon have nearly equal energy barriers, with the former slightly favored by 2.3 kcal mol^{-1}. In either case, a second dehydration should be facile because the barriers for these reactions are lower than the barriers for the first dehydration. For example, temperatures sufficient to surmount the first dehydration barriers of over 70 kcal mol^{-1} should be sufficient to overcome the barriers 60 kcal mol^{-1} or lower for the second dehydration. The second dehydration of 1,3-dihydroxypropene, **3**, is most likely to proceed through the pericyclic mechanism, because the barrier is over 30 kcal mol^{-1} lower than the 1,2-dehydration. Thus, the energetically favored product from 1,2-dehydration is acrolein, **7**, resulting from loss of the central hydroxyl followed by a pericyclic mechanism, whereas the formation hydroxy acetone, **11**, is also possible by a single 1,2-dehydration. High yields of acrolein have been measured[6,7] from glycerol pyrolysis, though no hydroxyacetone has been reported. It could be that this product further decomposes in the experimental procedure.

1,3-Dehydration. Loss of water from glycerol can also occur by the 1,3-dehydration shown in reaction 6. This pericyclic mechanism results in the loss of water and fragmentation to formaldehyde and vinyl alcohol. This reaction is endothermic with $\Delta_{react}E_{0K}$[reaction 6] = 25.4 kcal mol^{-1}. The structure of the transition state, **12**, is shown in Figure 1 and is consistent with the concerted formation of ethylene, formaldehyde, and water. The C1−C2 bond shortens from r_{C1-C2}(**3**) = 1.53 Å in glycerol to r_{C1-C2}(**12**) = 1.41 Å in the TS, the C3−O3 bond shortens from r_{C3-O3}(**3**) = 1.43 Å to r_{C3-O3}(**12**) = 1.30 Å, and the O1−H3 bond shortens from r_{O1-H3}(**3**) = 2.11 Å to r_{O1-H3}(**12**) = 1.05 Å. These bond lengths are close to the C=C, C=O and O−H bonds in ethylene, formaldehyde, and water. The other bonds in the ring elongate (C1−O1: r_{C1-O1}(**3**) = 1.43Å → r_{C1-O1}(**12**) = 2.12 Å, C2−C3: r_{C2-C3}(**3**) = 1.53 Å → r_{C2-C3}(**12**) = 1.83 Å, and O3−H3: r_{O3-H3}(**3**) = 0.97 Å → r_{O3-H3}(**12**) = 2.08 Å), indicating that these bonds are being broken. The calculated relative energy of the transition state is $\Delta_{TS}E_{0K}$[reaction 6] = 65.2 kcal mol^{-1}. The vinyl alcohol product from reaction 6 can tautomerize to form acetaldehyde, as is shown in reaction 7. The energy of this reaction is $\Delta_{react}E_{0K}$-[reaction 7] = −11.6 kcal mol^{-1} and the activation energy for the transition state is $\Delta_{TS}E_{0K}$[reaction 7] = 56.2 kcal mol^{-1}. These values compare well to values calculated[30] using the G1 method, $\Delta_{react}E_{0K}$[reaction 7] = −11.2 kcal mol^{-1} and $\Delta_{TS}E_{0K}$-[reaction 7] = 56.2 kcal mol^{-1}. Because the energy barrier for reaction 7 is lower than that for reaction 6, the formation of acetaldehyde should be facile at temperatures required for 1,3-dehydration.

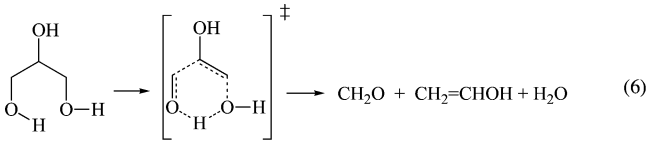

(6)

3 **12**

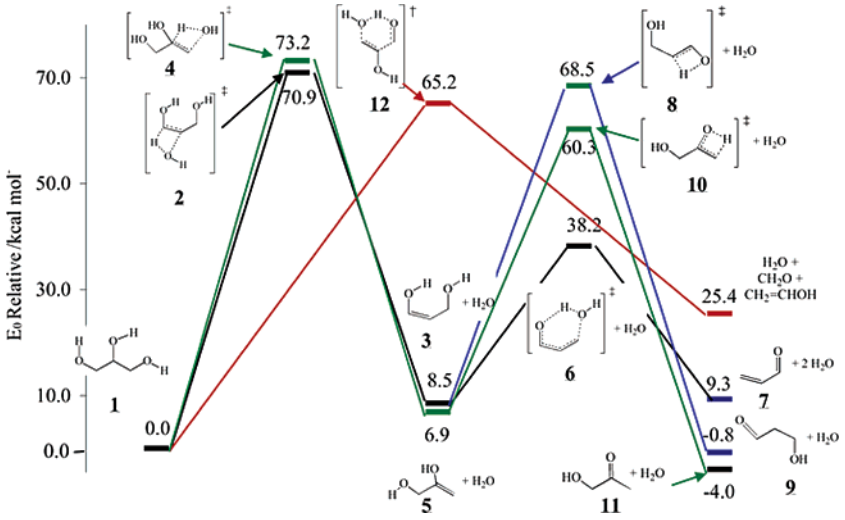

Figure 2. Potential energy plot for the reaction of neutral glycerol. Energies were determined with CBS-QB3 and include ZPE. (Black) Potential energy of reactions 1 and 3; (Green) potential energy of reactions 2 and 5; (Blue) potential energy of reactions 4; (Red) potential energy of reaction 6.

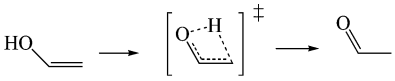
(7)

The potential energy plot for reaction 6 is shown in Figure 2. As can be seen, 1,3-dehydration has a slightly lower barrier than the 1,2-dehydration reactions. Thus, one would expect 1,3-dehydration products to also be important in pyrolysis. Experimental studies[6−8] have shown that acetaldehyde, a 1,3-dehydration product, is also a major product from glycerol pyrolysis. These results are also consistent with observations from pyrolysis GC−MS experiments using ^{13}C-labeled glycerol.[31]

Reactions of Protonated Glycerol. In protic solvents and in the presence of acid, glycerol can undergo proton catalyzed dehydration. In this study, the unimolecular decomposition of protonated glycerol was modeled by computing the energies of the reactants and transition states. Earlier computational[22] studies have shown that the activation barriers for the dehydration of protonated alcohols were lowered significantly relative to the neat alcohols, and one would expect there to be a similar enhancement for glycerol. This has been confirmed here, although the added hydroxyl groups present in glycerol result in additional dehydration pathways.

Protonation of glycerol can occur at either a terminal or the central hydroxyl group. The proton affinity for these two positions depends on the energy of the resulting conformer, with structures containing the most internal hydrogen bonds favored. For glycerol protonated at the terminal position, the lowest energy structure, **13**, has a cyclic hydrogen bonding geometry with the additional proton coordinated to the other terminal hydroxyl group, as shown in Figure 3. The calculated proton affinity for glycerol using this cation structure is *PA*(glycerol−O1) = 194.8 kcal mol^{-1}. This value is significantly higher than the experimental proton affinities of primary alcohols, *PA*(ethanol[32]) = 185.6 kcal mol^{-1}, and is likely due to additional coordination of the proton. This calculated value for glycerol is lower than the experimental value[33] for glycerol, *PA* = 201.7 kcal mol^{-1}, and 1,3-propane diol, *PA* = 203.9 kcal mol^{-1}, in which the two terminal hydroxyl groups also bind the proton.[34] The lowest-energy structure for protonation of glycerol at O2, **14**, is one in which the two hydrogen atoms on the central hydroxyl group are hydrogen bonded to the two terminal oxygen atoms. This structure is also shown in Figure 3, and the proton affinity connecting this conformer of glycerol is *PA*(glycerol−O2) = 195.4 kcal mol^{-1}. Thus, the proton affinities for the two distinct hydroxyl groups are nearly identical.

In this study, three dehydration mechanisms have been considered for protonated glycerol. A hydride transfer or pinacol mechanism is similar to the 1,2-dehydration mechanism discussed for neutral glycerol. A mechanism similar to the pericyclic mechanisms is also considered. Finally, substitution reactions are considered with one hydroxyl moiety acting as a nucleophile to displace water as the leaving and resulting in the formation of a cyclic ether.

Hydride Transfer (Pinacol Rearrangement). Dehydration of protonated glycerol can occur by a pinacol rearrangement in which there is a loss of H_2O at the site of protonation and a simultaneous shift of the adjacent hydride to the resulting carbocation. The hydride transfer reactions for glycerol protonated at O1 and O2 are shown in reactions 8 and 9, which result in the formation of protonated hydroxyacetone, **17**, or protonated 3-hydroxypropanal, **20**, respectively. The lowest-energy conformers for these species had internal hydrogen bonds, and the structures of these conformer are shown in Figure 3. The formation of these products is exothermic for reaction 8 with an energy of $\Delta_{react}E_{0K}$[reaction 8] = −7.2 kcal mol^{-1}, whereas reaction 9 is slightly endothermic, $\Delta_{react}E_{0K}$[reaction 9] = 0.4 kcal mol^{-1}. The 8 kcal mol^{-1} greater exothermicity of reaction 8 relative to reaction 9 is likely due to the observation that in **17**, the oxonium ion is bonded to a secondary carbon atom, whereas in **20**, the oxonium bonds to a primary carbon atom. The secondary carbon atom has a greater ability to distribute the charge, increasing its stability.

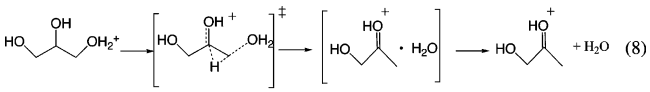
(8)

13 **15** **16** **17**

Because these reactions involve charged species in the gas phase, the unimolecular dissociation products, **17** or **20**, and the departing water molecule will experience a strong attractive ion−dipole potential. As a result, the initial products from dehydration are actually the water clusters **16** and **19**. In this study, no attempt is made to locate the global energy minima for all conformations of the clusters from dehydration. Likely

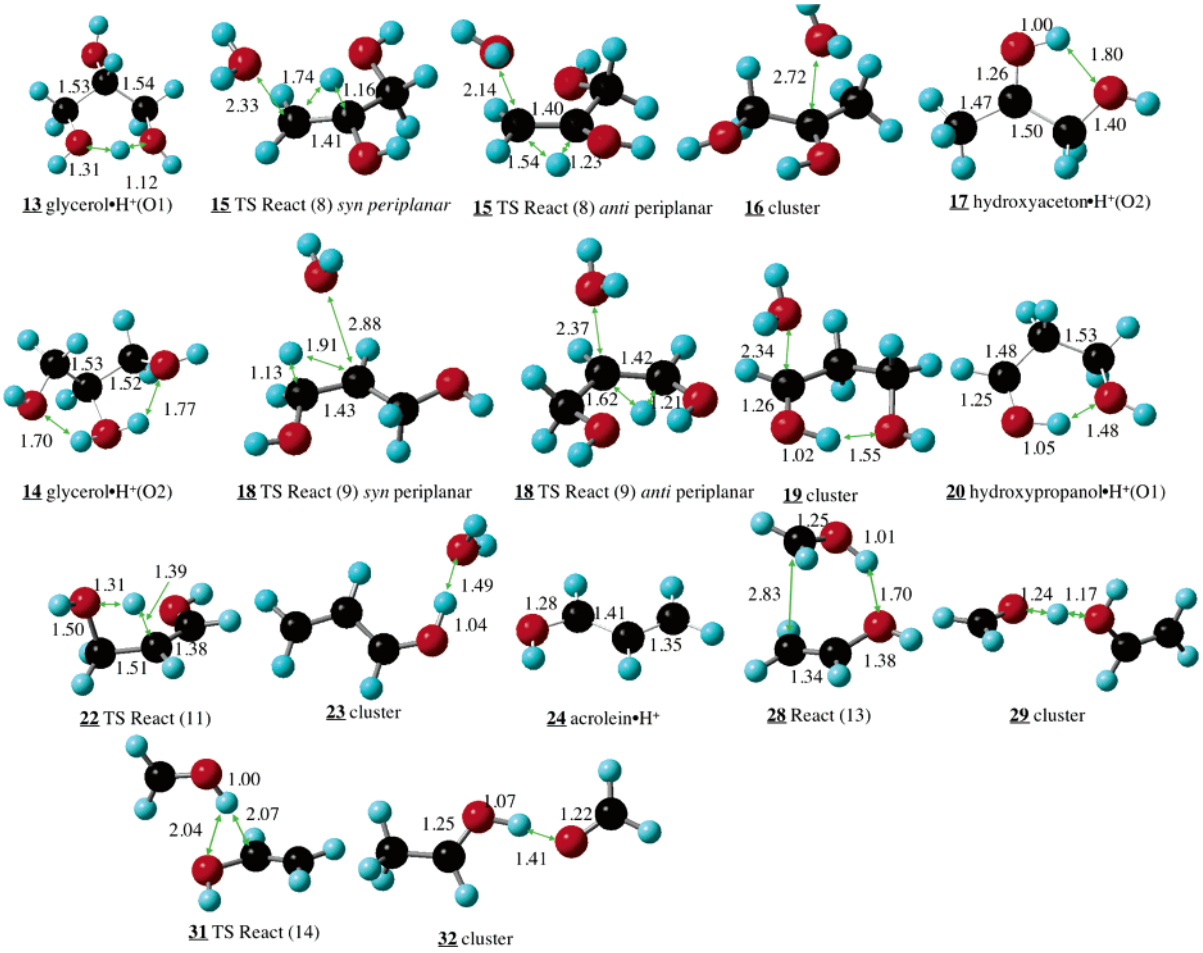

Figure 3. Selected bond lengths for the reactants, transition states, and products of reactions 8−16. Geometries were optimized using B3LYP/6-311G(d,p).

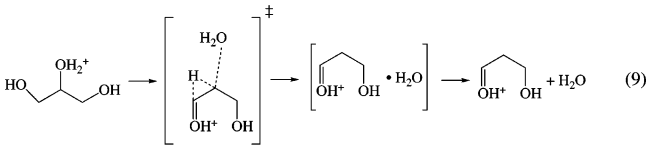

(9)

14 **18** **19** **20**

structures are chosen for illustrative purposes. Such structures of **16** and **19** are shown in Figure 3. For reaction 8, formation of the cluster is exothermic with an energy of $\Delta_{cluster}E_{0K}$[reaction 8] = −18.3 kcal mol^{-1}, whereas reaction 9 has an energy of $\Delta_{cluster}E_{0K}$[reaction 9] = −11.5 kcal mol^{-1}; thus, the cluster energies are approximately 11−12 kcal mol^{-1}. Note that in both cases, the electronegative oxygen of the water molecule is associated with the carbon atom attached to the oxonium ion, suggesting that this carbon atom contains significant positive charge. Mulliken charge distributions confirm this.

The transition states for hydride transfer can have either the *syn*- or *anti*-periplanar conformations with the hydride transfer occurring on the same side or the opposite side of the molecule with respect to the water loss. For example, the two transition states for the dehydration of glycerol protonated at O1 are shown below. It was found that the possible conformers of the *anti*-periplanar transition states were typically lower in energy than the corresponding conformers of the *syn*-periplanar transition states. Among the many conformers of the transition states calculated in this study, the lowest relative energy for glycerol protonated at O1 was $\Delta_{TS}E_{0K}$[reaction 8a] = 34.0 kcal mol^{-1} for the *syn*-periplanar transfer and $\Delta_{TS}E_{0K}$[reaction 8b] = 24.9 kcal mol^{-1} for *anti*-periplanar transfer (see Table 1). These barriers are consistent with the *anti* barriers calculated for propylene glycol,[16] E_a = 21.4, using B3LYP/6-31G(d) and ethylene glycol,[17] E_a = 24.4 kcal mol^{-1} using MP2/6-311G-(d,p)//MP2/6-311G(d). For protonation at O2, the lowest barriers found were $\Delta_{TS}E_{0K}$[reaction 9a] = 25.9 kcal mol^{-1} for *syn*-periplanar transfer and $\Delta_{TS}E_{0K}$[reaction 9b] = 22.4 kcal mol^{-1} for *anti*-periplanar transfer. The value for the *anti* conformer is consistent with the calculated barrier for propylene glycol,[16] E_a

TABLE 1: Reaction Energies[a] for the Dehydration of Protonated Glycerols

reaction	TS	cluster	products
Reaction of glycerol protonated at O1, *PA* = 194.8			
reaction 8a hydride transfer, *anti*-periplanar	24.9	−18.3	−7.2
reaction 8b hydride transfer, *syn*-periplanar	34.0	−18.3	−7.2
reaction 15 pericyclic reaction	36.2	2.5	52.8
reaction 17 protonated glycidol formation	21.4	9.7	32.8
reaction 18 protonated oxetane formation	24.9	4.2	26.7
Reactions of glycerol protonated at O2, *PA* = 195.4			
reaction 9a hydride transfer, *anti*-periplanar	22.4	−11.5	0.4
reaction 9b hydride transfer, *syn*-periplanar	24.6	−11.5	0.4
reaction 10 carbocation formation			36.9
reaction 19 protonated glycidol formation	25.2	10.0	33.1
reaction 11 second dehydration	36.1	−6.5	14.7
reaction 12 second dehydration C_4	21.7		
reaction 13 vinyl alcohol formation	20.7	11.9	40.6
reaction 14 acetaldehyde formation	12.0	−20.0	6.2

[a] Energies in kcal mol^{-1} are relative to the reactant and include zero-point energies.

= 18.7 kcal mol^{-1} from B3LYP/6-31G(d). The structures for these transition states (18-*syn* and 18-*anti*) are shown in Figure 3.

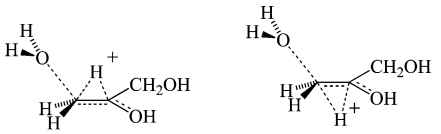

a. *syn* periplanar transfer **b. *anti* periplanar transfer**

As the name periplanar implies, the structures of these transition states are planar with respect to the leaving oxygen atom, both carbon atoms involved, and the H atom that is transferring. Interestingly, the sp^2 character of the two carbon atoms during the hydride transfer results in the formation of π-bonding character. This can be seen in the schematic below, which shows the bonding of the two carbon atoms in the reactant on the left, in the transition state in the middle, and in the product on the right. The C−C bond lengths are shown for the reaction of O1 with protonated glycerol. Both carbon atoms are sp^3 in the reactant, and the bond length is typical of a C−C single bond, r_{C-C} = 1.54 Å. In the transition state, both carbon atoms are sp^2 with a p-orbital involved in the hydride transfer. Because the transfer is a hydride, both p-orbitals must have the same sign. Thus, there is π-bonding character between these two atoms, as is shown by the short bond distance, r_{C-C} = 1.40 Å. This bonding was also confirmed by inspection of the HOMO of the transition state. Note that in the product, one of the carbon atoms is sp^3 hybridized and the bond has lengthened to r_{C-C} = 1.50 Å.

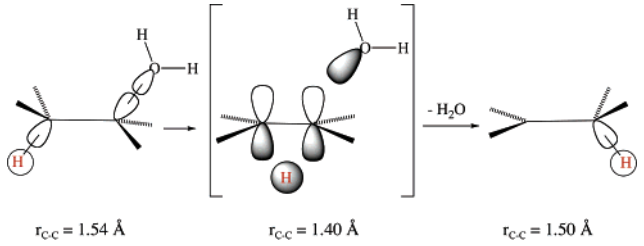

The hydride shift occurs simultaneously with water loss because the resulting protonated ketone is significantly more stable than the carbocation (reaction 10) that would result without concomitant hydride transfer. That is, reaction 10 is energetically disfavored compared with reaction 8 because **17** contains an oxonium ion, whereas **21** has a carbocation. This reasoning is consistent with the experimental proton affinity of propanal,[32] *PA*(CH_3CH_2CHO) = 187.9 kcal mol^{-1}, compared to that of propylene,[32] *PA*($CH_3CH{=}CH_2$) = 179.6 kcal mol^{-1}. The calculated endothermicity for reaction 10 is high, $\Delta_{react}E_{0K}$[reaction 10] = 36.9 kcal mol^{-1}. No transition state was located for this unimolecular dissociation, and stable structures of clusters could not be found, because the H_2O recombined with the carbocation. Potential energy scan calculations where the C2−O2 bond in **14** was sequentially stretched showed no potential energy barrier at the B3LYP/6-311G(d,p) level. Thus, it seems likely that this reaction is a simple barrierless bond scission with an activation energy equivalent to the reaction endothermicity (ca. 37 kcal mol^{-1}). This is significantly higher than the calculated activation energy for the hydride transfer mechanism discussed above. For glycerol protonated at O1, no carbocation was found, as all attempted geometry optimizations resulted in **17**.

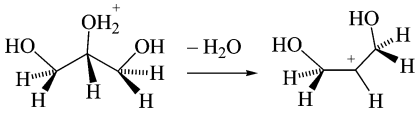

(10)

13 **21**

Of the products of hydride transfer, **17** and **20**, only protonated 3-hydroxypropanal, **20**, can readily undergo further dehydration. This step is a 1,2-dehydration, as shown in reaction 11. The product of this reaction is protonated acrolein, **24**, and the reaction is endothermic, $\Delta_{react}E_{0K}$[reaction 11] = 14.7 kcal mol^{-1}, but formation of the cluster is exothermic with an energy of $\Delta_{cluster}E_{0K}$[reaction 11] = −6.5 kcal mol^{-1}. The calculated energy barrier for this reaction is $\Delta_{TS}E_{0K}$[reaction 11] = 36.1 kcal mol^{-1}. The structures for the transition state of this reaction, the cluster, and the product are shown in Figure 3. Dehydration of **20** may also occur via a substitution mechanism such as the reverse of reaction 27 (see later). This substitution pathway has a barrier of 32.8 kcal mol^{-1} slightly lower than that predicted for the elimination reaction 11. Similar types of secondary dehydration are either not possible or unlikely for protonated hydroxyacetone, **17**.

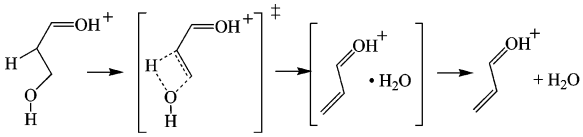

(11)

20 **22** **23** **24**

The barrier for reaction 11 is high compared to that for reaction 9, making this second dehydration unlikely for glycerol at moderate temperatures. For many sugars, this second dehydration would occur at a secondary carbon atom instead of a primary carbon atom, as shown in reaction 11. Dehydration of a secondary alcohol should be more facile. This reaction has been modeled by adding a methyl group to the hydroxyl bearing carbon atom of **20** to form a protonated hydroxy butanal, **25**, and the analogous reaction barrier was calculated for reaction 12. The structures of the reactant and the transition state for reaction 12 have been included in the Supporting Information. The calculated energy barrier for this reaction, $\Delta_{TS}E_{0K}$[reaction 12] = 21.7 kcal mol^{-1}, is low enough to be significant at moderate temperatures. Therefore, the double dehydration of protonated complex sugars appears likely to be facile.

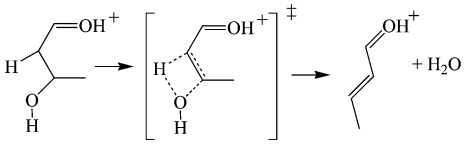

(12)

25 **26** **27**

Protonated 3-hydroxypropanal can also undergo a loss of formaldehyde to give protonated vinyl alcohol, as shown in reaction 13. This reaction is endothermic with an energy of $\Delta_{react}E_{0K}$[reaction 13] = 40.6 kcal mol^{-1} and a cluster formation energy of $\Delta_{cluster}E_{0K}$[reaction 13] = 11.9 kcal mol^{-1}. The structures for the species in reaction 13 are shown in Figure 3. As can be seen, the transition state for this reaction is essentially a cluster of vinyl alcohol with protonated formaldehyde, which is transferring a proton to the vinyl alcohol. The barrier for this reaction is $\Delta_{TS}E_{0K}$[reaction 13] = 20.7 kcal mol^{-1}.

The high endothermicity of reaction 13 also makes this reaction unlikely at moderate temperatures. However, formation

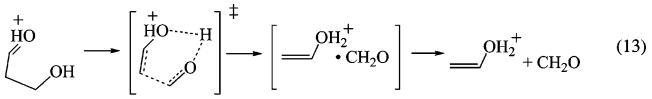

of protonated acetaldehyde, **33**, from the cluster, **29**, as shown in reaction 14 is possible. This reaction is only endothermic by 6.2 kcal mol^{-1}, compared to 29.0 kcal mol^{-1} for the formation of **30** from **29**. The barrier for reaction 14 is $\Delta_{TS}E_{0K}$[reaction 14] = 12.0 kcal mol^{-1}, and the formation of cluster **32** is $\Delta_{cluster}E_{0K}$[reaction 14] = −20.0 kcal mol^{-1} (see Figure 3). These results show that if C3 is a secondary carbon atom, loss of a second water molecule, reaction 12 is likely. If C3 is a primary carbon atom, formaldehyde loss, reaction 13 should occur.

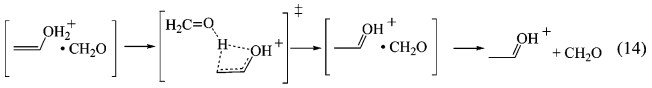

Pericyclic Dehydration. For glycerol protonated at O1, there is a pericyclic-like reaction as shown in reaction 15, which results in the formation of vinyl alcohol and protonated formaldehyde. However, the transition state for this reaction, **31**, does not involve an O1 to O3 hydrogen transfer. Instead, this reaction is a concerted loss of water and protonated formaldehyde. The barrier for reaction 15 is $\Delta_{TS}E_{0K}$[reaction 15] = 36.2 kcal mol^{-1}. Because this is high compared to the barriers for hydride transfer, this reaction is unlikely to be significant. The cluster in this reaction contains protonated formaldehyde, vinyl alcohol, and water, and the structure is shown in Figure 4. The energy to form this cluster is $\Delta_{cluster}E_{0K}$-[reaction 15] = 2.5 kcal mol^{-1}, whereas the energy of reaction 15 is ΔE_{0K}[reaction 15] = 27.7 kcal mol^{-1}.

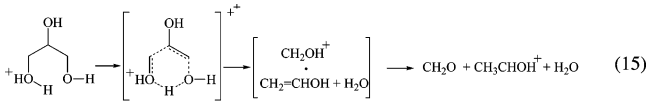

The transition state for pericyclic dehydration of glycerol protonated at O2, such as is shown in reaction 16 could not be located.

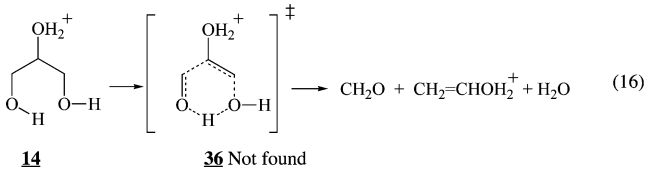

Substitution. The unprotonated hydroxyl groups of glycerol can displace the $-OH_2^+$ group on protonated glycerol by substitution reactions to form cyclic products. For glycerol protonated at O1, **13**, substitution by the O2 hydroxyl group forms a protonated glycidol, **39**, reaction 17, whereas substitution by the O3 hydroxyl group forms protonated 3-hydroxyoxetane, **42**, reaction 18. For glycerol protonated at O2, **14**, only the glycidol can be formed, as shown in reaction 19. The structures of these two cyclic, substitution products are shown in Figure 5. The C−C bond length in the epoxide ring of the glycidol r_{C-C}(**39**) = 1.46 Å and is similar to the experimental value measured[35] for neutral ethylene oxide, r_{C-C}(ethylene

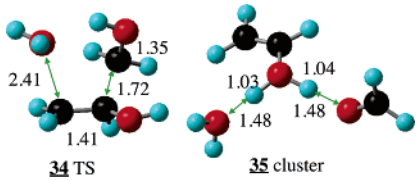

Figure 4. Selected bond lengths for the transition state, **34**, and the cluster products from the pericyclic dehydration of glycerol using B3LYP/6-311G(d,p).

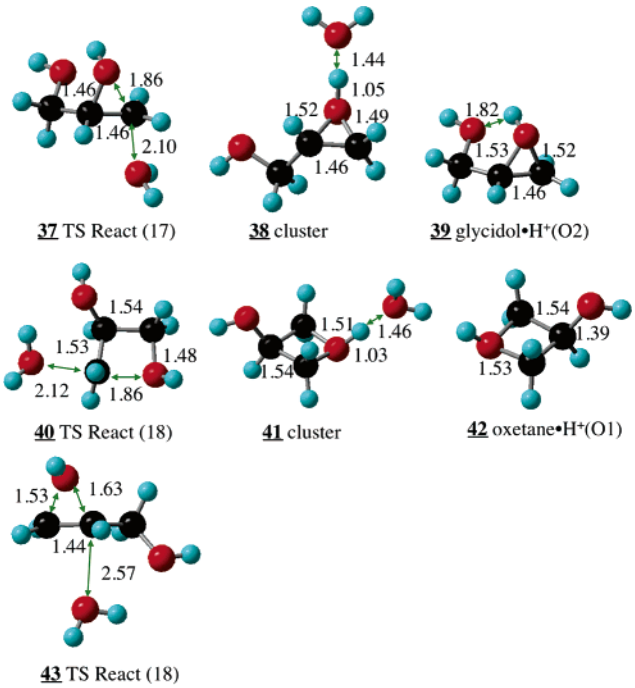

Figure 5. Selected bond lengths for the transition states for the formation of protonated glycidol from protonated glycerol, **37** and **43**, and the transition state for the formation of protonated hydroxy oxetane, **40**. The geometries of the water cluster products are shown, **38** and **41**, as are the dehydrated protonated products, **39** and **42**. Geometries were optimized at B3LYP/6-311G(d,p).

oxide) = 1.459 Å. The C−O epoxide bonds, r_{C-O}(**39**) = 1.52 Å and r_{C-O}(**39**) = 1.53 Å, are longer than those bonds in ethylene oxide, r_{C-O}(ethylene oxide) = 1.425 Å, which is probably a result of protonation on the ring oxygen atom. Similarly, in **42**, the C−C bond lengths, r_{C-C}(**42**) = 1.54 Å, are consistent with experimental[36] values of neutral oxetane, r_{C-C}(oxetane) = 1.543 Å, whereas the C−O bonds are longer, r_{C-O}(**42**) = 1.53 Å and r_{C-O}(oxetane) = 1.446 Å. Note that **42** has C_2 symmetry, so both C−O and C−C bonds are the same length.

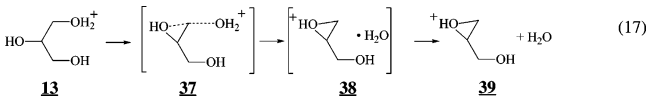

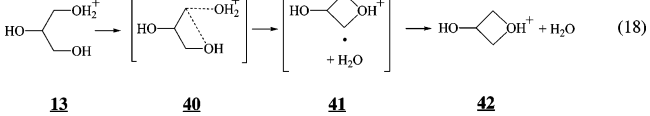

Though the formation of these cyclic ethers are endothermic processes, the barriers are low enough that these dehydration pathways are energetically accessible. Formation of the cluster, **38**, from glycerol protonated at O1 by reaction 17 is endothermic by $\Delta_{cluster}E_{0K}$[reaction 17] = 9.7 kcal mol^{-1}, whereas formation

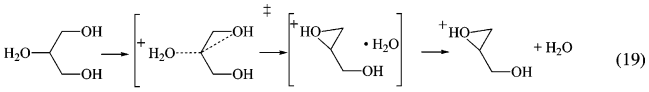

(19)

14 **43** **38** **39**

of the separated products is quite endothermic with ΔE_{0K}[reaction 17] = 32.8 kcal mol^{-1}. Formation of the oxetane cluster, **41**, in reaction 18 is endothermic by $\Delta_{cluster}E_{0K}$[reaction 18] = 4.2 kcal mol^{-1}, and the energy for reaction 18 is ΔE_{0K}[reaction 18] = 26.7 kcal mol^{-1}. The reaction of glycerol protonated at O2, as shown in reaction 19, is endothermic for the formation of the cluster with an energy of $\Delta_{cluster}E_{0K}$[reaction 19] = 10.0 kcal mol^{-1}, whereas the energy for complete reaction to separated products is ΔE_{0K}[reaction 19] = 33.1 kcal mol^{-1}. For both the protonated glycidol and hydroxyoxetane, the complexation energy for a water molecule is high (23.1 and 22.5 kcal mol^{-1}, respectively). This high value is presumably due to the observation that the charge on these species cannot be delocalized through the molecule as it can with the products from the hydride transfer reactions, **17** and **20**, for example. The activation barrier for reaction 17 is $\Delta_{TS}E_{0K}$[reaction 17] = 21.4 kcal mol^{-1}, whereas for reaction 18 and 19 the barriers are $\Delta_{TS}E_{0K}$[reaction 18] = 24.9 kcal mol^{-1} and $\Delta_{TS}E_{0K}$[reaction 19] = 25.2 kcal mol^{-1}. The barriers for reactions 17 and 19 are similar to the calculated barrier for the formation of protonated ethylene oxide from ethylene glycol, E_a = 24.4 kcal mol^{-1}, using MP2/6-311G(d,p)//MP2/6-311G(d). The barrier for the formation of protonated hydroxy oxetane, reaction 18, is significantly lower than that calculated for the formation of protonated oxetane from 1,3-propane diol,[17] E_a = 32.7 kcal mol^{-1}, using MP2/6-311G(d,p)//MP2/6-311G(d). This barrier is about 8 kcal mol^{-1} higher than the calculated barrier for glycerol. Perhaps this difference is due to hydrogen bonding between the leaving water molecule and the middle hydroxyl group. These energy barriers suggest that reaction 17 is most likely, but the other pathways have barriers close enough that they may also be significant.

Further reaction of protonated glycidol and 3-hydroxyoxetane are also possible. The glycidol, **39**, can undergo a substitution reaction to form the 3-hydroxyoxetane, **42**, by reaction 20, and thus, these two reaction channels are linked. This chemistry is analogous to the gas phase rearrangements of the corresponding alkoxide anions observed by Bowie and co-workers.[37] Reaction 20 is nearly thermo-neutral, ΔE_{0K}[reaction 20] = 1.6 kcal mol^{-1} with an energy barrier of $\Delta_{TS}E_{0K}$[reaction 20] = 27.6 kcal mol^{-1}. The structure for this transition state is shown in Figure 6. The calculated potential energy surface for the further reaction of the protonated glycidol is shown in Figure 7. The glycidol can end up as a vinylmethyl ether cation, **49**, plus a water molecule or protonated acetaldehyde, **33**, plus formaldehyde. Figure 8 shows the calculated reaction pathways for the hydroxyoxetane. The hydroxyoxetane can end up as a oxetane cation, **59**, or protonated acetaldehyde, **33**.

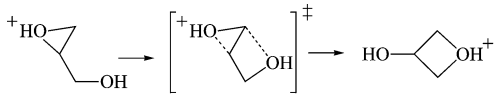

(20)

39 **44** **42**

Vinylmethyl ether cation, **49**, can be formed from glycidol by a proton transfer, which is reaction 21 followed by a concerted ring opening and dehydration, reaction 22. Reaction 21 is endothermic, ΔE_{0K}[reaction 21] = 17.1 kcal mol^{-1}, with a barrier of $\Delta_{TS}E_{0K}$[reaction 21] = 21.3 kcal mol^{-1}. Formation of the cluster in reaction 22 is exothermic, $\Delta_{cluster}E_{0K}$[reaction 22] = −16.2 kcal mol^{-1}, whereas the energy of the separated products is ΔE_{0K}[reaction 22] = −4.0 kcal mol^{-1} and with an activation barrier of just $\Delta_{TS}E_{0K}$[reaction 22] = 9.4 kcal mol^{-1}. Note that the energy required to dissociate the water cluster, **48**, to give the ether cation and water is low, 12.2 kcal mol^{-1}, because of the delocalization of the charge in the cation. The structures for **45**−**49** are shown in Figure 6. In the transition state for proton transfer, **45**, the proton is closer to the primary oxygen atom, O1, than it is to the ring oxygen atom, Or, r_{O1-H} = 0.97 Å and r_{Or-H} = 3.23 Å, indicating that this is a late transition state. This is consistent with the transition state being closer in energy to the product than the reactant. Because the barrier for reaction 22 is much higher than the barrier for the reverse of reaction 21, $\Delta_{TS}E_{0K}$[reverse of reaction 21] = 21.3−17.1 = 4.2 kcal mol^{-1}, the overall reaction to form **49** will be inefficient and dependent upon the steady-state concentration of **46**. However, Figure 7 shows that this still remains the lowest-energy exit channel for protonated glycidol. Other isomeric forms of **49** may also be possible.

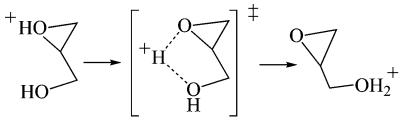

(21)

39 **45** **46**

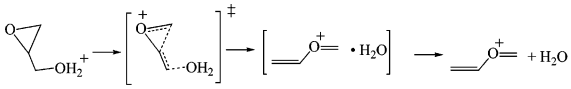

(22)

46 **47** **48** **49**

In the cluster from reaction 22, the water molecule can add across the ends of the ether, as shown in reaction 23, and the product can further decompose to protonated acetaldehyde and formaldehyde, reaction 24. The structures for these species are also shown in Figure 6. The transition state for reaction 23, **50**, is a six-membered ring, which accounts for the low barrier, $\Delta_{TS}E_{0K}$[reaction 23] = 10.3 kcal mol^{-1}. In the transition state for reaction 24, protonated formaldehyde has dissociated from the acetaldehyde fragment and is in the process of transferring a proton back to the acetaldehyde. The barrier for this step, $\Delta_{TS}E_{0K}$[reaction 24] = 12.9 kcal mol^{-1}, can be overcome with the addition of the exothermicity of reaction 23, ΔE_{0K}[reaction 23] = −19.1 kcal mol^{-1}. Thus, this reaction channel should be facile once the water cluster, **48**, is formed.

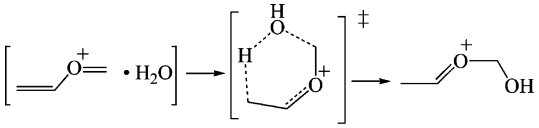

(23)

48 **50** **51**

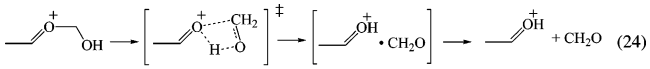

(24)

51 **52** **32** **33**

The 3-hydroxyoxetane can also undergo a proton transfer, reaction 25, followed by dehydration, reaction 26, to form the oxetane cation, **57**. The structures of **53**−**57** are shown in Figure 6. Reaction 25 is endothermic with an energy of ΔE_{0K}[reaction 25] = 15.0 kcal mol^{-1} and a barrier of $\Delta_{TS}E_{0K}$[reaction 25] = 19.7 kcal mol^{-1}. The dehydration step is a hydride transfer reaction similar to those in reactions 8 and 9. By direct analogy,

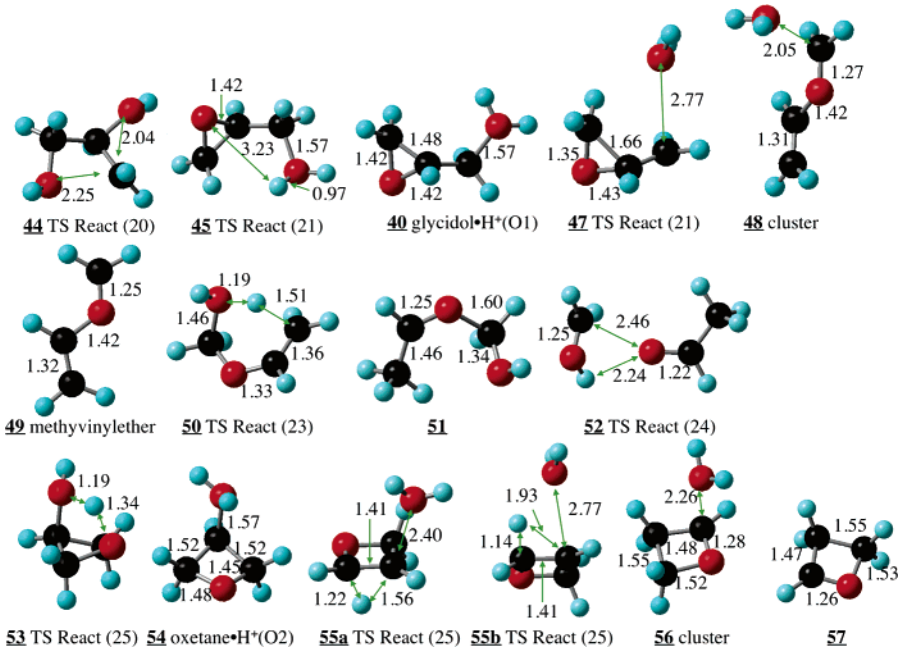

Figure 6. Selected bond lengths for transition states and products from the reactions of protonated glycidol and 3-hydroxyoxetane determined using B3LYP/6-311G(d,p).

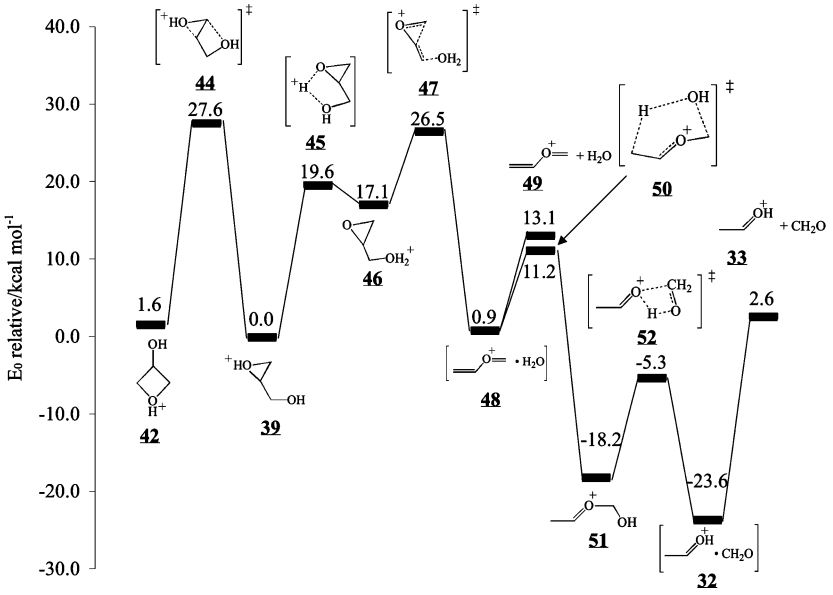

Figure 7. Relative potential energies, including ZPE, of the possible reactions protonated glycidol, **39**.

syn- and *anti*-periplanar conformations of the transition states were located, and both are shown in Figure 6. Note that the C−C bond involved in the hydride transfer also shortens in the transition state relative to the reactant and product. For the *anti*-periplanar transition state, the bond length is r_{C-C} (**54**) = 1.52 Å in the hydroxyoxetane, r_{C-C} (**55a**) = 1.41 Å in the *anti*-periplanar transition state, and r_{C-C} (**57**) = 1.55 Å for the product oxetane cation. This also shows the double-bond character of the transition state. Once again, the *anti*-periplanar transition state is lower in energy than the *syn*-periplanar transition state, $\Delta_{TS}E_{0K}$[reaction 26, anti] = 16.8 kcal mol^{-1} and $\Delta_{TS}E_{0K}$[reaction 26, syn] = 18.8 kcal mol^{-1}. The cluster formation energy for reaction 26 is −23.7 kcal mol^{-1}, whereas the energy of the reaction to form the separated products is ΔE_{0K}[reaction 26] = 7.8 kcal mol^{-1}.

As with the protonated glycidol, the oxetane cation/water cluster can also undergo a water addition to the oxetane cation, as is shown in reaction 27. In this case, the reaction produces

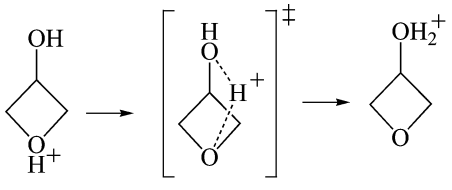

(25)

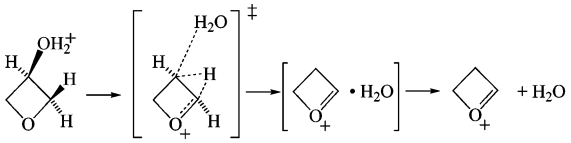

(26)

3-hydroxypropanal, **20**, which is also the product of the hydride transfer reaction shown in reaction 9. This reaction is exother-

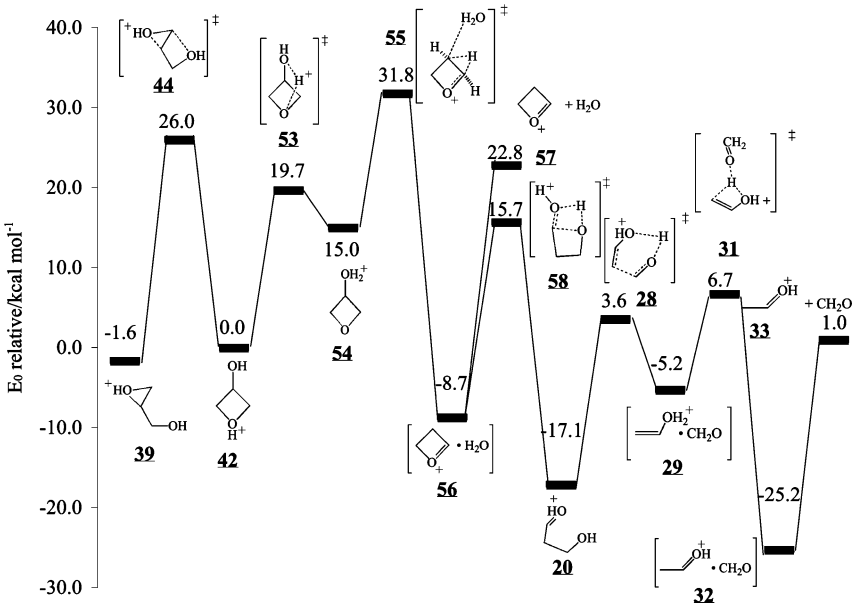

Figure 8. Relative potential energies, including ZPE, of the possible reactions of protonated 3-hydroxyoxetane, **42**.

mic, ΔE_{0K}[reaction 27] = −8.4 kcal mol^{-1}, with a barrier of, $\Delta_{TS}E_{0K}$[reaction 27] = 24.4 kcal mol^{-1}. The hydroxypropanal could react further, as shown in reactions 13 and 14, to give formaldehyde and protonated acetaldehyde, **33**. Recall that the barriers for these reactions were $\Delta_{TS}E_{0K}$[reaction 13] = 20.7 kcal mol^{-1} and $\Delta_{TS}E_{0K}$[reaction 14] = 12.0 kcal mol^{-1}. As with glycidol, the exothermicity from reaction 26 should help surmount these barriers.

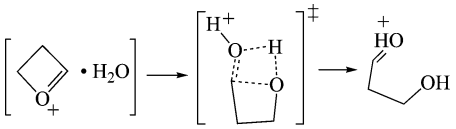

(27)

56 **58** **20**

The results of these calculations suggest that protonated glycidol, **39**, and protonated 3-hydroxyoxetane, **42**, should react further by dehydration or loss of formaldehyde. The reaction of both species will be dependent upon the proton transfer and loss of water to form the complex that can be seen in Figures 7 and 8. Because the proton transfer step is significantly endothermic, the reaction will be limited by the pseudoequilibrium concentration of the proton-transfer products, **46** and **54**. Once the water cluster is formed, the subsequent reactions should be facile because sufficient internal energy will be generated from surmounting the barriers for reactions 22 and 26. This can be seen in Figures 7 and 8, which show that these barriers are higher than the barriers for subsequent reactions.

Figure 9 collects all of the reaction mechanisms for protonated glycerol considered in this study. This scheme shows the activation energy for each step and the masses of the products are shown.

Mass Spectrometry Experiments. Mass spectrometry provides a critical tool for the investigation of the unimolecular behavior of ions in the gas phase. In this study, protonated glycerol was introduced into the gas phase by electrospray ionization of an acidified aqueous acetonitrile solution. The resultant ions were mass selected and subjected to collision induced dissociation (CID) in a triple−quadrupole mass spectrometer. The CID spectrum of protonated glycerol (*m*/*z* 93) is shown in Figure 10a and reveals a prominent fragment ion at *m*/*z* 75 corresponding to the loss of a water molecule in line with theoretical predictions. Other fragment ions observed are also consistent with calculation, including *m*/*z* 57, which arises from sequential loss of two water molecules, and *m*/*z* 45, which arises from loss of water and formaldehyde. Ions observed at low mass include *m*/*z* 29, protonated formaldehyde, and *m*/*z* 19, the hydronium cation, both of which can be rationalized as forming by intracomplex proton transfer following unimolecular dissociation. All calculations predict that the loss of formaldehyde should arise exclusively from the terminal carbons, and indeed, this prediction was borne out by ^{13}C-labeling experiments (see caption to Figure 10).

The *m*/*z* 75 fragment ion in the CID spectrum of protonated glycerol corresponds to an elemental composition of $C_3H_7O_2^+$, which may correspond to any of the isomeric structures previously discussed or indeed a mixture of isomers (e.g., **17**, **20**, **39**, **42**, **46**, and/or **54**). For comparison, the CID mass spectrum of one of these isomers, protonated glycidol, was obtained and is presented in Figure 10b. The spectrum is very similar to the corresponding mass range in the spectrum of protonated glycerol with all the same fragment ions observed. This is hardly a surprising observation given that calculation suggests that dissociation of protonated glycidol will be preceded by isomerization (see Figure 7), and thus, the activated *m*/*z* 75 ion populations are likely to be similar mixtures of isomers and give very similar fragments. Interestingly, both spectra show a similar abundance in the *m*/*z* 57 fragment ion compared to *m*/*z* 75, which suggests that for protonated glycerol, the former ion arises from secondary fragmentation of the latter. This interpretation is consistent with calculation, which found numerous pathways for consecutive water loss but no mechanism for concerted loss of two water molecules. In contrast, however, the ion abundance of *m*/*z* 45 in the glycidol spectrum (Figure 10b) is somewhat lower than for the same ion in the glycerol spectrum (Figure 10a). This might suggest a significant contribution of a mechanism accounting for concomitant loss of water and formaldehyde, such as predicted for the pericyclic reaction 13. Overall, the mass spectrometric data can be rationalized in terms of the computed reaction mechanisms.

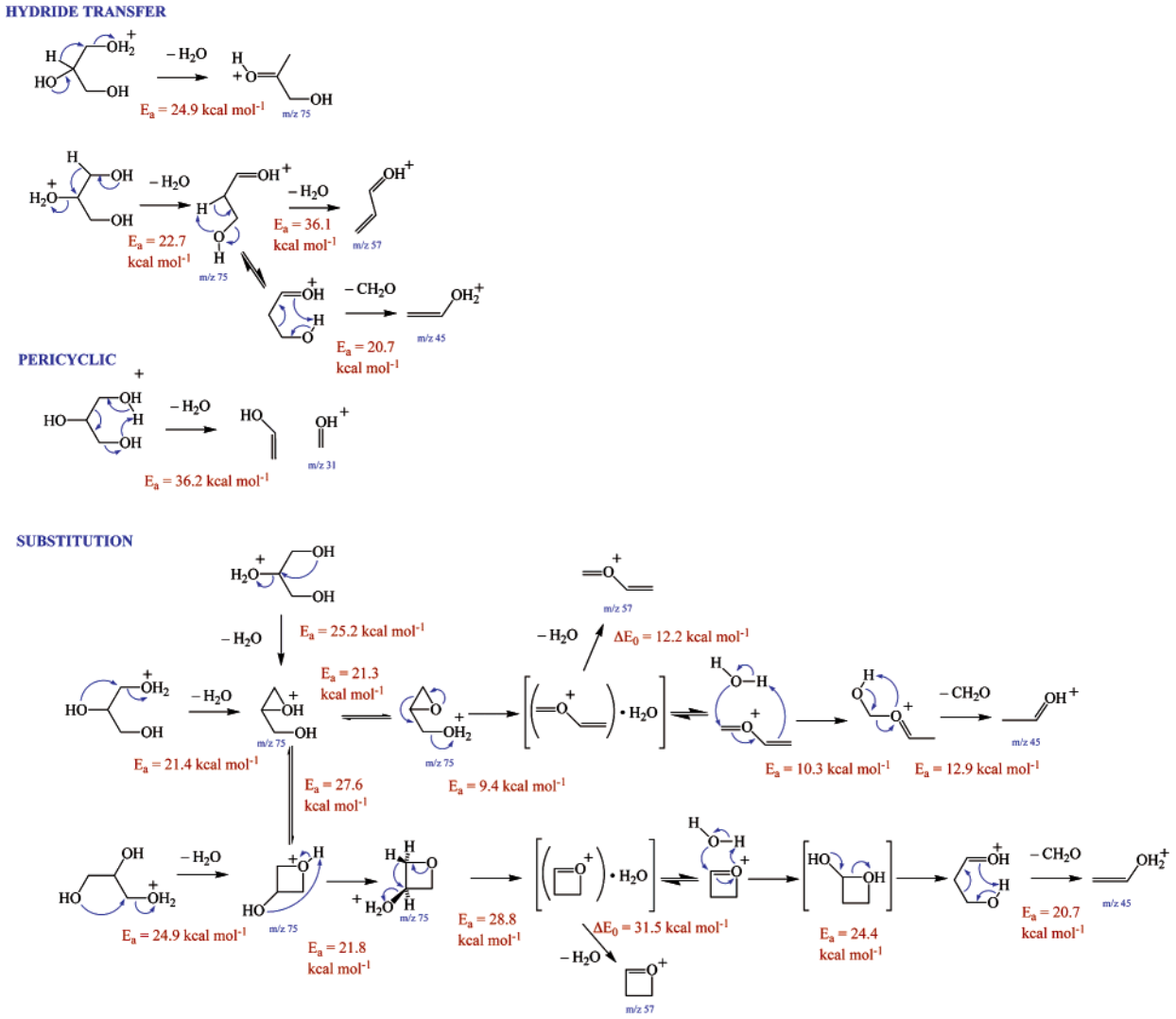

Figure 9. Reaction mechanisms for the dehydration of protonated glycerol. Activation energies, E_a, were determined using CBS-QB3.

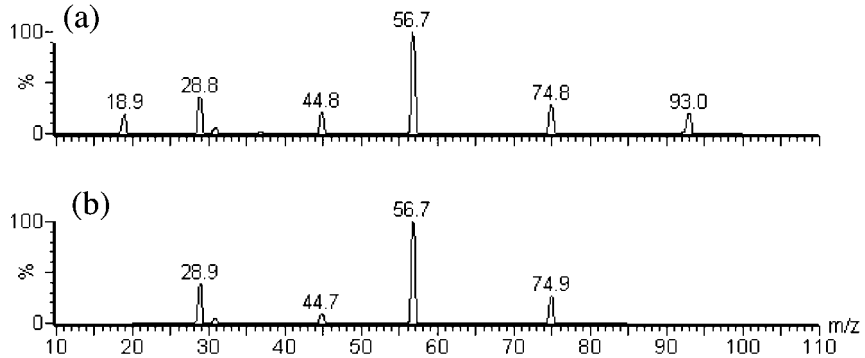

Figure 10. (a) CID mass spectrum of protonated glycerol measured on a Waters QuattroMicro triple quadrupole mass spectrometer. The corresponding spectrum for ^{13}C-2-glycerol gives ions at *m*/*z* 94, 76, 58, and 46, whereas $^{13}C_2$-1,3-glycerol gives ions at *m*/*z* 95, 77, 59, and 46. (b) CID mass spectrum of protonated glycidol measured under the same conditions.

Conclusions

Calculations of the dehydration of glycerol by the neutral mechanisms explored here indicate that these processes can only occur at relatively high temperatures such as are found in pyrolysis or combustion. The addition of acids will allow substantially lower dehydration temperatures. The hydride transfer and substitution reactions discussed here for protonated glycerol have barriers that are between 21 and 25 kcal mol^{-1} and are susceptible to decomposition at much lower temperatures. Thus, these types of reactions should become important in industrial processes involving triols, such as sugars.

Acknowledgment. The Department of Energy Office of the Biomass Program provided funding for this work. We would also like to acknowledge support from the National Computational Science Alliance, grant number CHE980028N, and from the Computational Sciences Center at the National Renewable Energy Center for computational cycles.

Supporting Information Available: Calculated structures of the reactants, transition states, and products. This material is available free of charge via the Internet at http://acs.pubs.org.

References and Notes

(1) *Chemicals and Materials from Renewable Resources*; Bozell, J. J., Ed.; American Chemical Society: Washington, 2001; Vol. 784.

(2) *Feedstocks for the Future Renewables for the Production of Chemical and Materials*; Bozell, J. J., Patel, M. K., Eds.; American Chemical Society: Washington, 2005; Vol. 921.

(3) *Wood and Cellulosic Chemistry*; Hon, D. N. -S., Shiraishi, N., Eds.; Marcel Dekker: New York, 1990.

(4) *Handbook on Bioethanol: Production and Utilization*; Wyman, C. E., Ed.; Taylor and Francis: Washington, 1996.

(5) *Fuels and Chemicals from Biomass*; Saha, B. C., Woodward, J., Eds.; American Chemical Society: Washington, 1997; Vol. 666.

(6) Antal, M. J.; Mok, W. S. L.; Roy, J. C.; Raissi, A. T.; Anderson, D. G. M. *J. Anal. Appl. Pyrolysis* **1985**, *8*, 291.

(7) Stein, Y. S.; Antal, M. J.; Jones, M. *J. Anal. Appl. Pyrolysis* **1983**, *4*, 283.

(8) Buhler, W.; Dinjus, E.; Ederer, H. J.; Kruse, A.; Mas, C. *J. Supercrit. Fluids* **2002**, *22*, 37.

(9) Ramayya, S.; Brittain, A.; Dealmeida, C.; Mok, W.; Antal, M. J. *Fuel* **1987**, *66*, 1364.

(10) Antal, M. J.; Leesomboon, T.; Mok, W. S.; Richards, G. N. *Carbohydr. Res.* **1991**, *217*, 71.

(11) Feather, M. S. *Tetrahedron Lett.* **1970**, *48*, 4143.

(12) Feather, M. S.; Harris, D. W.; Nichols, S. B. *J. Org. Chem.* **1972**, *37*, 1606.

(13) Harris, D. W.; Feather, M. S. *Carbohydr. Res.* **1973**, *30*, 359.

(14) Hurd, C. D.; Isenhour, L. L. *J. Am. Chem. Soc.* **1932**, *54*, 317.

(15) Smith, W. B. *Tetrahedron* **2002**, *58*, 2091.

(16) Rungnim, C.; Ruangpornvisuti, V. *J. Comput. Chem.* **2005**, *26*, 1592.

(17) Bouchoux, G.; Choret, N.; Flammang, R. *J. Phys. Chem. A* **1997**, *101*, 4271.

(18) Frisch, M. J.; Trucks, G. W.; Schlegel, H. B.; Scuseria, G. E.; Robb, M. A.; Cheeseman, J. R.; Zakrzewski, V. G.; Montgomery, J. A., Jr.; Stratmann, R. E.; Burant, J. C.; Dapprich, S.; Millam, J. M.; Daniels, A. D.; Kudin, K. N.; Strain, M. C.; Farkas, O.; Tomasi, J.; Barone, V.; Cossi, M.; Cammi, R.; Mennucci, B.; Pomelli, C.; Adamo, C.; Clifford, S.; Ochterski, J.; Petersson, G. A.; Ayala, P. Y.; Cui, Q.; Morokuma, K.; Malick, D. K.; Rabuck, A. D.; Raghavachari, K.; Foresman, J. B.; Cioslowski, J.; Ortiz, J. V.; Stefanov, B. B.; Liu, G.; Liashenko, A.; Piskorz, P.; Komaromi, I.; Gomperts, R.; Martin, R. L.; Fox, D. J.; Keith, T.; Al-Laham, M. A.; Peng, C. Y.; Nanayakkara, A.; Gonzalez, C.; Challacombe, M.; Gill, P. M. W.; Johnson, B. G.; Chen, W.; Wong, M. W.; Andres, J. L.; Head-Gordon, M.; Replogle, E. S.; Pople, J. A. *Gaussian 98*, revision ; Gaussian, Inc.: Pittsburgh, PA, 1998.

(19) Frisch, M. J.; Trucks, G. W.; Schlegel, H. B.; Scuseria, G. E.; Robb, M. A.; Cheeseman, J. R.; Montgomery, J. A., Jr.; Vreven, T.; Kudin, K. N.; Burant, J. C.; Millam, J. M.; Iyengar, S. S.; Tomasi, J.; Barone, V.; Mennucci, B.; Cossi, M.; Scalmani, G.; Rega, N.; Petersson, G. A.; Nakatsuji, H.; Hada, M.; Ehara, M.; Toyota, K.; Fukuda, R.; Hasegawa, J.; Ishida, M.; Nakajima, T.; Honda, Y.; Kitao, O.; Nakai, H.; Klene, M.; Li, X.; Knox, J. E.; Hratchian, H. P.; Cross, J. B.; Bakken, V.; Adamo, C.; Jaramillo, J.; Gomperts, R.; Stratmann, R. E.; Yazyev, O.; Austin, A. J.; Cammi, R.; Pomelli, C.; Ochterski, J. W.; Ayala, P. Y.; Morokuma, K.; Voth, G. A.; Salvador, P.; Dannenberg, J. J.; Zakrzewski, V. G.; Dapprich, S.; Daniels, A. D.; Strain, M. C.; Farkas, O.; Malick, D. K.; Rabuck, A. D.; Raghavachari, K.; Foresman, J. B.; Ortiz, J. V.; Cui, Q.; Baboul, A. G.; Clifford, S.; Cioslowski, J.; Stefanov, B. B.; Liu, G.; Liashenko, A.; Piskorz, P.; Komaromi, I.; Martin, R. L.; Fox, D. J.; Keith, T.; Al-Laham, M. A.; Peng, C. Y.; Nanayakkara, A.; Challacombe, M.; Gill, P. M. W.; Johnson, B.; Chen, W.; Wong, M. W.; Gonzalez, C.; Pople, J. A. *Gaussian 03*, revision C.02; Gaussian, Inc.: Wallingford, CT, 2004.

(20) Foresman, J. B.; Frisch, A. E. *Exploring Chemistry with Electronic Structure Methods*, 2nd ed.; Gaussian, Ind.: Pittsburgh, 1995.

(21) Hodgson, D.; Zhang, H. Y.; Nimlos, M. R.; McKinnon, J. T. *J. Phys. Chem. A* **2001**, *105*, 4316.

(22) Nimlos, M. R.; Blanksby, S. J.; Ellison, G. B.; Evans, R. J. *J. Anal. Appl. Pyrolysis* **2003**, *66*, 3.

(23) Basch, H.; Hoz, S. *J. Phys. Chem. A* **1997**, *101*, 4416.

(24) Bach, R. D.; Glukhovtsev, M. N.; Gonzalez, C.; Marquez, M.; Estevez, C. M.; Baboul, A. G.; Schlegel, H. B. *J. Phys. Chem. A* **1997**, *101*, 6092.

(25) Montgomery, J. A.; Frisch, M. J.; Ochterski, J. W.; Petersson, G. A. *J. Chem. Phys.* **1999**, *110*, 2822.

(26) Nimlos, M. R.; Filley, J.; McKinnon, J. T. *J. Phys. Chem. A* **2005**, *109*, 9896.

(27) Callam, C. S.; Singer, S. J.; Lowary, T. L.; Hadad, C. M. *J. Am. Chem. Soc.* **2001**, *123*, 11743.

(28) Lewis, D.; Keil, M.; Starr, M. *J. Am. Chem. Soc.* **1974**, *96*, 4398.

(29) Tsang, W. *Int. J. Chem. Kinet.* **1976**, *8*, 173.

(30) Smith, B. J.; Nguyen, M. T.; Bouma, W. J.; Radom, L. *J. Am. Chem. Soc.* **1991**, *113*, 6452.

(31) Paine, J. B., III.

(32) Hunter, E. P. L.; Lias, S. G. *J. Phys. Chem. Ref. Data* **1998**, *27*, 413.

(33) Bouchoux, G.; Djazi, F.; Gaillard, F.; Vierezet, D. *Int. J. Mass Spectrom.* **2003**, *227*, 479.

(34) Bouchoux, G.; Berruyer-Penaud, F. *J. Phys. Chem. A* **2003**, *107*, 7931.

(35) Kuchitsu, K. *Structure Data of Free Polyatomic Molecules*; Springer-Verlag: New York, 1995; Vol. 23.

(36) Hellwege, K. H.; Hellwege, A. M. E. *Structure Data of Free Polyatomic Molecules*; Springer-Verlag: Berlin, 1976; Vol. 7.

(37) Dua, S.; Taylor, M. S.; Buntine, M. A.; Bowie, J. H. *J. Chem. Soc., Perkin Trans.* **1997**, *2*, 1991.